Fatigue crack initiation detection by an infrared thermography method

D. Wagner, Nicolas Ranc, Claude Bathìas, Paul C. Paris

Fatigue crack initiation detection by an infrared thermography method

D. WAGNER[1], N. RANC[2], C. BATHIAS[1] and P.C. PARIS[3]

[1]*LEME, Université Paris X, 50 rue de Sèvres - 92410 Ville D'Avray, France,* [2]*L.M.S.P., UMR CNRS 8106, Arts et Métiers Paris Tech, 151, boulevard de l'Hôpital, 75013 Paris, France,* [3]*LAMEFIP EA 2727, Arts et Métiers, Esplanade des Arts et metiers, 33405 Talence Cedex, France*

Received in final form 22 October 2009

ABSTRACT In this paper, the study of the temperature variation during fatigue tests was carried out on different materials (steels and aluminium alloys). Tests were performed at ambient temperature using a piezoelectric fatigue system (20 kHz). The temperature field was measured on the surface of the specimen, by means of an infrared camera.

Just at the beginning of the test, it was observed that the temperature increased, followed by a stabilization which corresponds to the balance between dissipated energy associated with microplasticity and the energy lost by convection and radiation at the specimen surface and by conduction inside the specimen. At the crack initiation, the surface temperature suddenly increases (whatever the localization of the initiation), which allows the determination of the number of cycles at the crack initiation and the number of cycles devoted to the fatigue crack propagation. In the gigacycle fatigue domain, more than 92% of the total life is devoted to the initiation of the crack.

So, the study of the thermal dissipation during the test appears a promising method to improve the understanding of the damage and failure mechanism in fatigue and to determine the number of cycles at initiation.

Keywords infrared pyrometry; number of cycles at crack initiation; temperature recording; very high cycle fatigue.

NOMENCLATURE

b = burger vector
E = Young's modulus
K_{eff} = effective stress intensity factor
K = stress intensity factor
$\Delta\sigma$ = stress amplitude
σ_y = yield stress
σ'_y = cyclic yield stress

INTRODUCTION

In fatigue tests, according to the strain or stress level, three domains exist. For few number of cycles at fracture ($N_f < 10^4$ cycles), it is the low cycle fatigue domain; for intermediate number of cycles at fracture ($10^4 < N_f < 10^7$ cycles), it is the high cycle fatigue domain (megacycle domain) and for high number of cycles at fracture ($N_f > 10^7$ cycles), it is the very high cycle fatigue domain (gigacycle domain).[1] The latter domain is now investigated with the development of devices (piezoelectric fatigue machines) working at high frequency (20 or 30 kHz), allowing to obtain 10^8 or more cycles in reasonable tests time. These tests have shown that fracture can occur at 10^9 or more cycles which is problematic because many components and structures in several industries require design fatigue life often superior to 10^8 cycles.

At a macroscopic scale, according to the fatigue domain, different types of crack initiation occur in cylindrical samples with a polished surface depending on whether it is low cycle, mega or giga-cycle fatigue range. For the smallest number of cycles at failure, the initiation sites are multiple and located on the surface. For intermediate number of cycles at failure, there is only one surface initiation site, whereas in gigacycle fatigue domain, the initiation site may be located in an internal zone or at the surface.

At the microscopic level, Mugrahbi et al.[2] show that the initiation of fatigue crack in the gigacycle fatigue regime

Correspondence: D. Wagner. E-mail: daniele.wagner@u-paris10.fr

can be described in terms of microstructurally irreversible portion of the cumulative cycle strain. It seems that there is no basic difference between fatigue mechanisms in low, mega and giga-cycle fatigue except for the strain localization. For the low cycle fatigue, an important plastic deformation of the specimen bulk governs the initiation. In the megacycle fatigue, the plastic deformation is governed by the plane stress effect and the presence of flaws at the surface which is the critical location of fatigue initiation. However, at lower stress, the plastic deformation in plane stress condition is vanishing and the macroscopic behaviour of the metal is fully elastic except around flaws, metallurgical defects or inclusions. As the probability of occurrence of a flaw is greater in a volume than at a surface, it is normal that the initiation site in gigacycle fatigue will be often in subsurface. In this case, the important parameters are the defect size and the position of the defect. When the initiation is located on an internal defect, the crack propagation leads to a fish-eye propagation around the defect. The geometry of the fish-eye initiation is a circle that collapses on reaching the surface of the specimen. In an internal initiation, it is difficult to determine the number of cycles at initiation. To predict the number of cycles to initiate a fatigue crack from an inclusion, several models are used more or less successfully.[1] In the gigacycle fatigue range, the integration of Paris' law[3–5] allows one to predict the number of cycles in the fish-eye growth and obtain the number of cycles at crack initiation. As the crack initiation appears, a short crack around the defect propagates followed by a long crack. In all cases, a cyclic plastic zone around the crack exists. During fatigue cycles, the irreversible part of the rate of the plastic work is responsible for the intrinsic dissipation. When the crack initiation occurs, the plastic deformation at the crack tip increases, and the recording of the surface temperature of the sample during the test allows to follow the crack propagation and to determine the number of cycles at the crack initiation.[6]

In the literature, the infrared pyrometry was already used by many authors,[7–16] but it is the dissipation before the crack initiation which was investigated. Often, the purpose was to get a rapid estimation of the fatigue limit by recording the temperature during the beginning of the test on fatigue machines working at low frequency. To further in number of cycles, the duration of the tests was prohibitive.

In this study, we investigate the temperature evolution measured by an advanced infrared imaging system on various materials between 10^5 and 10^8 cycles on a piezoelectric fatigue system at the frequency of 20 000 Hz. In this case, the duration of the test is compatible with the storage of the data in the camera and allows the recording of the temperature during the crack propagation.

Table 1 Mechanical properties and fatigue test conditions

Alloy	UTS (MPa)	*R* ratio	Stress amplitude (MPa)
AlSi7Mg06	344	0.01	52.5
			50
			45
AlSi5Cu3Mg	222	−1	55
AISI 4240 ($T = 430\ ^\circ$C)	1508	−1	460
AISI 4240 ($T = 610\ ^\circ$C)	1035	−1	345
AISI 5120	2000	−1	335

EXPERIMENTAL CONDITIONS

Materials

Two cast aluminium–silicon alloys (an AlSi7Mg06 and an AlSi5Cu3Mg) and three low alloyed steels (two 42CrMo4 or AISI 4240 and a bearing steel AISI 5120) were studied. The aluminium alloys differed by the composition (silicon amount . . .), and the two AISI 4240 steels by the heat treatment. Both the low alloyed AISI 4240 steels were austenized at 830 °C during 30 min, oil quenched but one was tempered during 1 h at 430 °C and the second one at 610 °C.

The differences result in various Yield Stress and Ultimate Tensile Stress (Table 1). The cast aluminium alloys showed a characteristic dentritic microstructure with porosities and the low alloyed steels a martensitic microstructure.

The experimental mechanical properties of these alloys and the fatigue test conditions (stress amplitude) of the materials are given in Table 1. These alloys have been tested at 20 kHz using a piezoelectric fatigue system with different *R* ratio (Table 1).

The specimens from AISI 4240 were prepared to be transversal (*T*) with respect to the rolling direction.

Experimental fatigue tests

From an historical point of view, the first ultrasonic fatigue machine was constructed in 1950 by Mason.[17] With the development of computer techniques, C. Bathias and co-workers[18,19] have built a fully computer-controlled piezoelectric fatigue machine working at 20 ± 0.5 kHz. Figure 1 shows the principal aspect of this machine in which the following three components are present:

- A power generator that transforms 50 or 60 Hz voltage signal into ultrasonic 20 kHz electrical sinusoidal signals.
- A piezoelectric (or magnetostrictive) transducer excited by the power generator, which transforms the electrical signal into longitudinal ultrasonic waves and mechanical vibration of the same frequency.

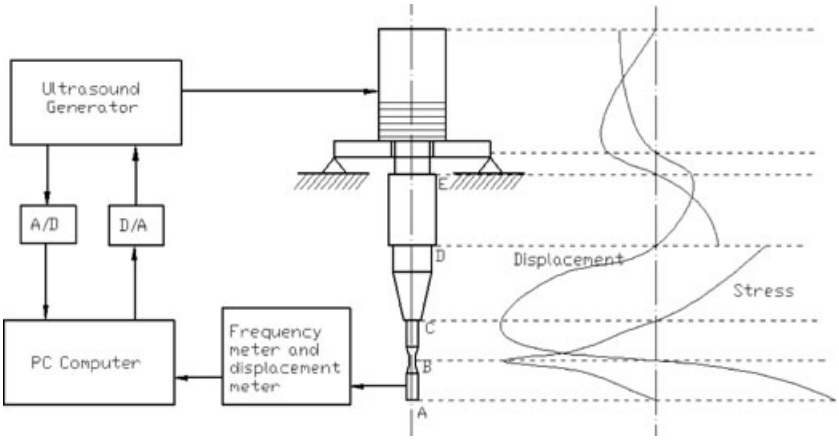

Fig. 1 Scheme of the piezoelectric fatigue machine.

- An ultrasonic horn (in titanium alloy, portion EDC in Fig. 1) that amplifies the vibration coming from the transducer in order to obtain the required strain amplitude in the middle section of the specimen. This amplifier maintains automatically the intrinsic frequency of the mechanical system in the range 19.5–20.5 kHz. Depending on the specimen loading, the horn is designed so that the displacement is amplified between *E* and *C* usually three to nine times. It means that the geometry of the horn must be determined. The finite element method may be required when the geometrical shape is complex.

The resonant length of the specimen and concentrator is calculated using Finite Element Method (FEM) by Ansys code. The converter, horn and specimen compose a mechanical vibration system where there are four stress nodes (null stress) and three displacement nodes (null displacement for an intrinsic frequency of 20 kHz) (Fig. 1). During the test, these nodes don't move and remain around at the same position and even damage occurs, because the crack remains small compared to the specimen size.

In our machine, in order to keep the stress constant, during the test, via computer control, there is:

- a linear relation between the electric potential and the dynamic displacement amplitude of the ceramic.
- a linear relation between dynamic displacement amplitude of the ceramic and displacement amplitude of the horn.
- a linear relation between displacement amplitude of the horn and electric potential.

The dynamic displacement amplitude at the horn extremity and at the specimen extremity is measured by an optic fibre sensor, which permits measurements of the displacement from 1 to 199.9 μm, with a resolution of 0.1 μm. During ultrasonic fatigue tests, the maximum strain values can be measured directly using miniature strain gauges, suitably positioned on the sample surface. The macroscopic pure homogeneous elastic behaviour during the test (except the case of plastic instabilities dues to phase transformations . . . , the change of yield stress during the test . . .) allows the determination of the dynamic Young's modulus of the tested material. To avoid this use of a load sensor, once the knowledge of the dynamic modulus is achieved, the stress in the mid-section of the specimen is computed from the displacement of the piezo-ceramics system after calibration. When a crack initiates, the dynamic modulus decreases and the device cannot maintain the required frequency (19.5–20.5 kHz), and the test is automatically stopped when the frequency falls below 19.5 kHz. The uncertainty is given by the ratio 0.5/20 which corresponds to minus 2.5% of error.

Temperature measurement

In order to determine the temperature field on the surface of the specimen, a nonintrusive measurement technique by infrared pyrometry was chosen. In the test, an advanced, high-speed and high-sensitivity infrared camera from Cedip Infrared Systems (made up of a matrix of 320 × 240 Mercury Cadmium Telluride detectors) was used to record the temperature changes during ultrasonic fatigue tests. The spectral range of the camera lies between 3.7 and 4.9 μm. This method allows the visualization of temperature cartography with very good time resolution. In this study, the spatial resolution is 0.17 mm and the aperture time can vary between 10 μs (two cycles) and 1500 μs (around 30 cycles). The refresh time of the camera is between 0.83 and 100 Hz. It corresponds respectively to a noise of 0.4 K and 20 mK. The pyrometer was calibrated on a blackbody reference. In pyrometry, the error in temperature is often related to uncertainties on the emissivity of the surface. To eliminate this problem, the specimen surface was covered with a strongly emissive black paint. Figure 2 shows our experimental device.

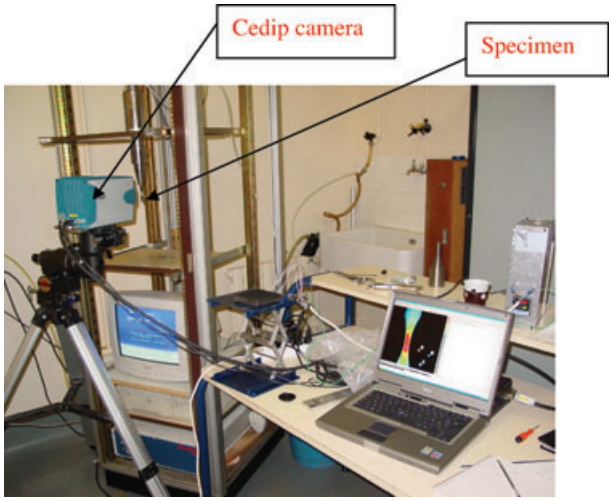

Fig. 2 Thermal measurement device.

RESULTS

Thermal results

Figures 3a and 4a show the temperature variation at the centre of the specimen as a function of the number of cycles for different stress levels in the case of a cast aluminium–silicon alloy (AlSi7Mg06) and a low alloyed steel (AISI 4240). The result for the AISI 5120 is given in Ref. [6]. The global behaviour is the same for all studied alloys.

At the first time, we observe an increase of the temperature just at the beginning of the test. In the same material, the temperature increases depending on the maximum stress amplitude for a given number of cycles. It should be noted that this increase in temperature at the beginning of the test is followed by a stabilization corresponding to a balance between the mechanical energy dissipated and the energy lost by convection and radiation at the specimen surface and by conduction inside the specimen. The temperature variation depends on the material and on stress amplitude level ($\Delta\sigma$) for a same material. Table 2 gives the maximum temperature variation (ΔT) obtained just before fracture, and N_f the number of cycles at fracture. The number of cycles at fracture was between 3×10^5 and 8×10^7 cycles, which is in the mega and gigacycle fatigue domain.

An enlargement of the experimental results at the failure is represented in Figs 3b (corresponding to the test with $\Delta\sigma = 52.5$ MPa) and 4b. From the thermographies of the specimens recorded by the camera during the fatigue tests, the point with the highest temperature is found. It is at this point that the evolution of the temperature variation versus the number of cycles is drawn. The behaviour is the same for all studied materials. At the end of the test, there is a local and abrupt increase of the temperature. It is shown that this rapid increase in temperature before failure is related to a very local increase of the temperature (thermographies of Figs 3c and 4c). The waypoints marked on the graph in Figs 3b and 4b correspond to the captured pictures in Figs 3c and 4c.

Fracture surface analysis

Scanning Electron Microscopy (SEM) was performed for fracture surface analysis in order to determine the origin and localization of the initiation (Table 2). In all materials, the initiation of the crack was initiated on inclusions (steels) or porosities (cast aluminium alloys). Figures 5 and 6 show the crack initiation zone on the fracture surface in the cast aluminium alloy AlSi5Cu3Mg and the bearing steel AISI 5120 where the initiation was subsurface. In the steel, the initiation was on a non-metallic inclusion and leads to a typical fish-eye propagation whereas in the cast aluminium alloy, it is on a porosity. In this case, the fracture crack growth is circular around the porosity and produces like a fish eye.

DISCUSSION

H. Mughrabi[2] has studied for many years the microstructural evolution of different materials during fatigue tests. He proposed to distinguish two kinds of materials which correspond at two extreme materials: the type I material is a ductile single-phase material without inclusions and the type II material is high-strength steel containing non-metallic inclusions. For the two types, the *S–N* curve can be described in a multi-stage Wöhler-type *S–N* plot where there are four ranges characterized by:

(I) the LCF (Low Cycle Fatigue domain) Coffin Manson range.
(II) the PSB (Permanent Slip Bands) threshold related to the HCF (High Cycle Fatigue or mega cycle domain) plastic strain fatigue limit.
(III) the transition from HCF limit to the UHCF range (gigacycle fatigue domain)
(IV) the irreversibility threshold corresponding to the UHCF limit.

Whatever the fatigue range, glide of dislocations are observed in the matrix. The microstructural evolution is always the same and leads to local plastic deformation and thus to mechanical energy dissipated into heat.

When inclusions (or porosities are present) in the case of type II materials, subsurface fatigue crack initiation at inclusions is dominant in the UHCF range III,[1,2] provided that the inclusion density lies below a critical value.[2] It is now accepted that in this case,[1] the total lifespan is mainly consumed by the process of crack initiation.

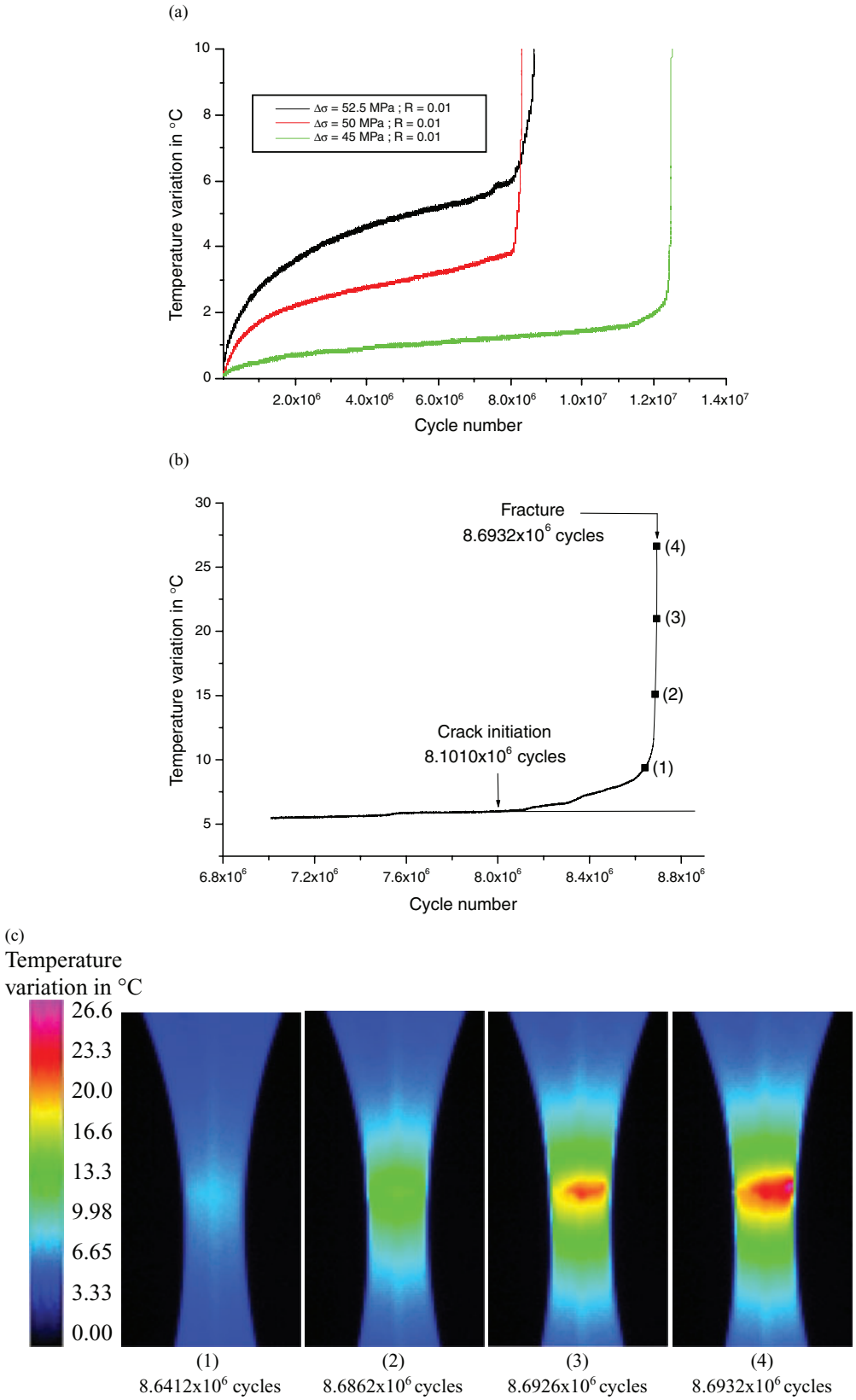

Fig. 3 Evolution of the temperature variation for the AlSi7 Mg06 alloy.

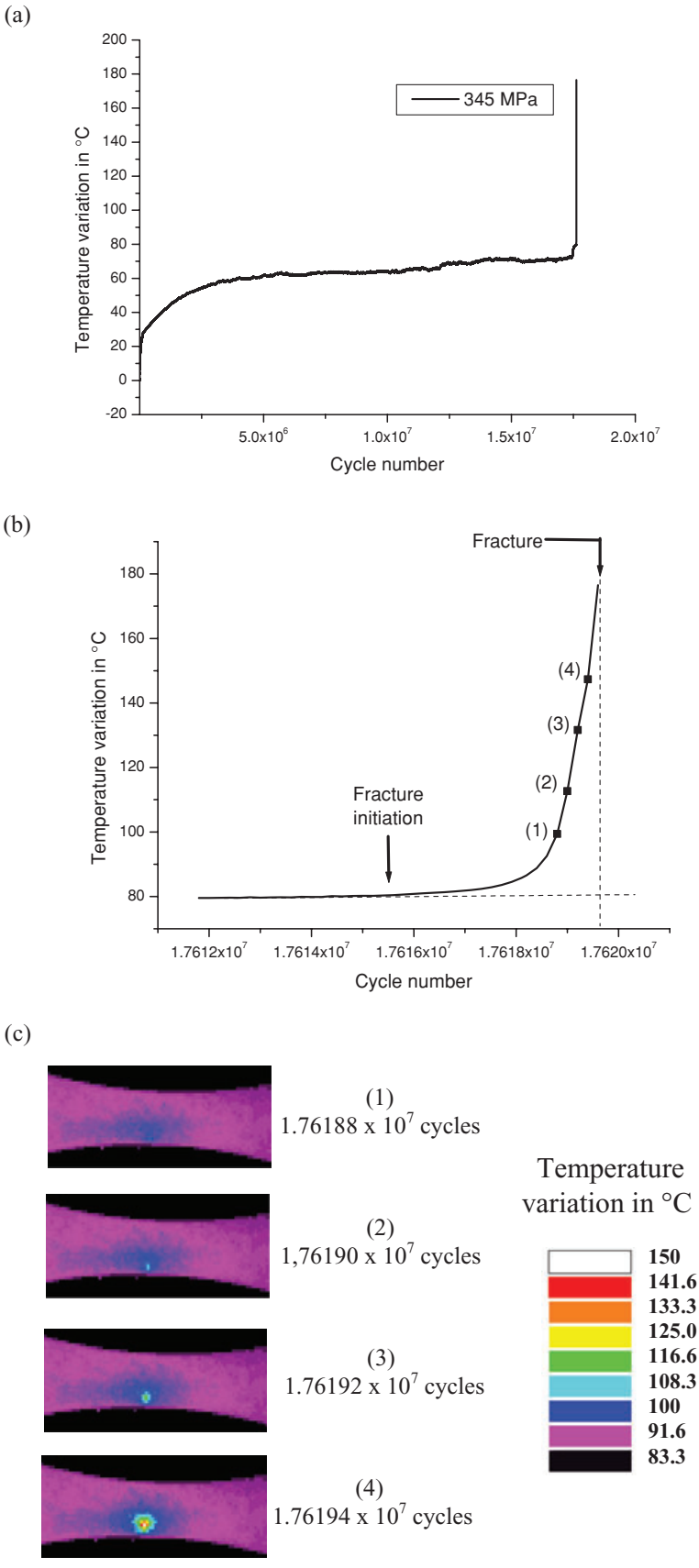

Fig. 4 Evolution of the temperature variation during the test for AISI 4240 steel ($T = 610\ ^{\circ}\text{C}$, $\Delta\sigma = 345$ MPa).

Table 2 Results of fatigue tests

Alloy	$\Delta\sigma$ (MPa)	ΔT (°C)	N_f	Localization
AlSi7Mg06	52.5	5.2	8.6932×10^6	Surface
	50	3.8	8.3276×10^6	
	45	1.3	1.25132×10^7	
AlSi5Cu3Mg	50	14	8.11392×10^7	Subsurface
AISI 4240 ($T = 430$ °C)	460	28	3.3094×10^5	Surface
AISI 4240 ($T = 610$ °C)	345	80	1.76197×10^7	Surface
AISI 5120	335	230	8.3700×10^7	Subsurface

When the crack is initiated, two plastic zones exist at the root of the crack:[20] the monotonic plastic zone $r_y = K^2/6\pi\sigma_y^2$ and the reverse (cyclic) plastic zone $r_R = \Delta K^2/24\pi\sigma_y'^2$ in which the plastic deformation is more intense (with σ_y, the yield stress, σ_y', cyclic yield stress and K, the stress intensity factor). When the crack initiates from a defect, such as inclusions or pores, it is said that probably a relation must exist between the fatigue limit and the crack growth threshold;[1,2,21] and the propagation of the crack in the fish eye can be modelled by the Paris–Hertzberg law[3] $da/dN = b(\Delta K_{eff}/Eb^{1/2})^3$ with E Young's modulus, b the Burger vector, K_{eff} effective stress intensity factor. In the first approach, the integration of this law without transition short crack–long crack from a_o to a the radius of the fish eye (Fig. 7) conducts[4] to $N_{prop} = \pi E^2/2\Delta\sigma^2$ with N_{prop} number of cycles for the propagation of the fish eye, $\Delta\sigma$ the experimental nominal stress and $a_o = a_{int}/0.94$ (a_{int}, radius of the defect: inclusion, . . .).

In our experiments, the temperature fields on the specimen surface are measured by infrared thermography. Just before the fracture, thermographies show a significant

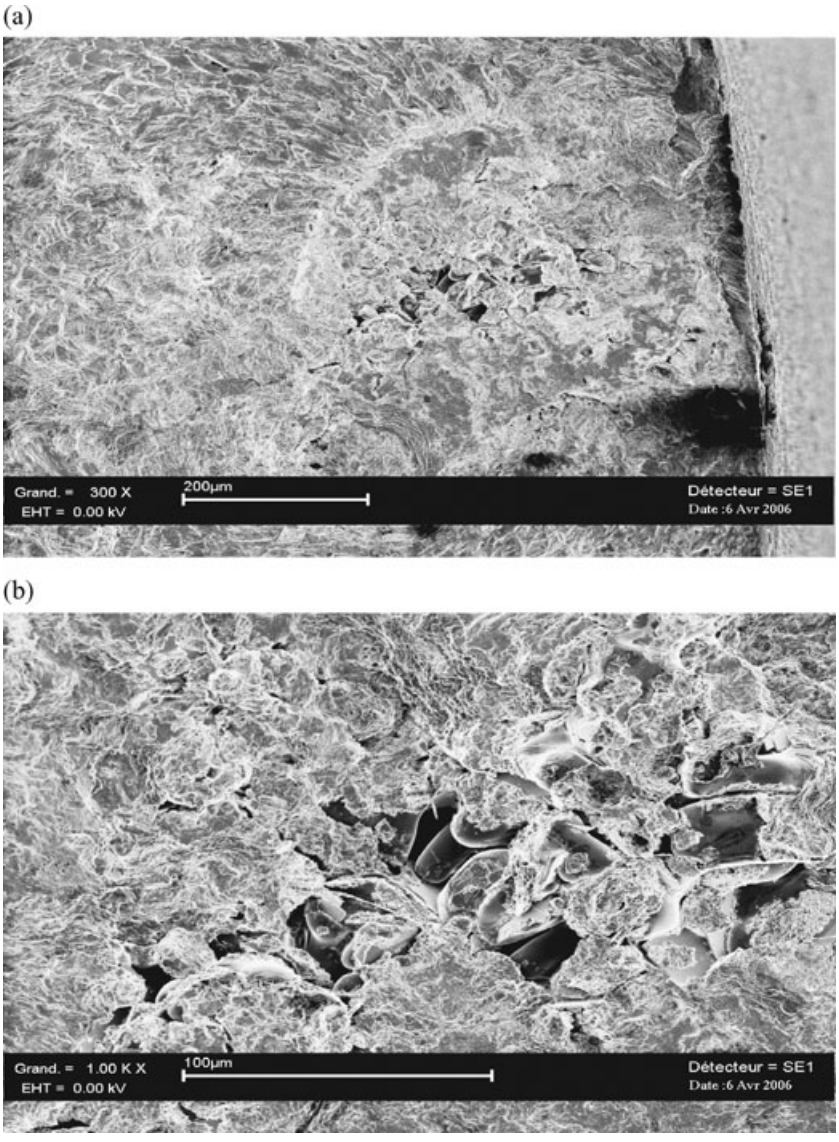

Fig. 5 (a) Crack initiation zone in the AlSi5Cu3 Mg alloy. (b) Detail of the crack initiation zone in the AlSi5Cu3 Mg alloy.

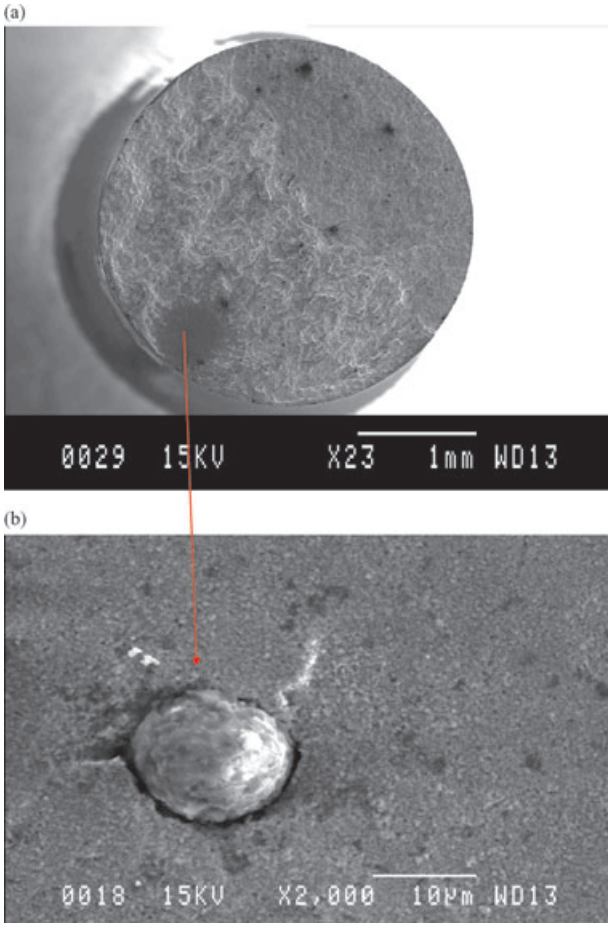

Fig. 6 (a) Fracture surface of the AISI 5120 steel (with fish eye). (b) Non-metallic inclusion in the fish eye in the AISI 5120 steel[6].

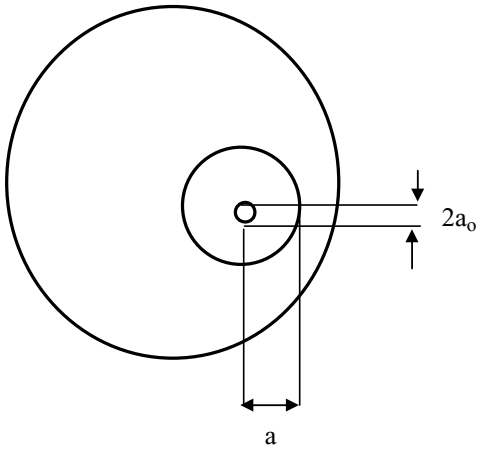

Fig. 7 Modelling of fish eye.

and local increase in the temperature. In order to better understand these thermal effects and to make a connection with the initiation and the propagation of the fatigue crack, a thermo-mechanical model was developed

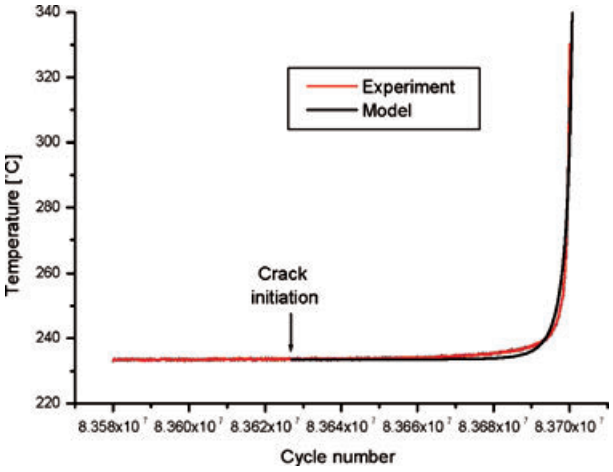

Fig. 8 Comparison between model and experiment for crack initiation detection (AISI 5120)[6].

for the bearing steel.[6] From the Paris–Hertzberg law, the evolution of crack length versus time can be obtained: $a(t) = a_0/(1-t/t_c)^2$ with $t_c = 2a_0/bf$ (with f the loading frequency).

Besides, the energy dissipated at each cycle per unit of crack length noted ξ is proportional to the surface of the reverse plastic zone r_R: $\xi = \eta r_R^2$ where η is a coefficient depending only on the material properties. By replacing the expression of r_R, ΔK and $a(t)$, the dissipated power per unit length of crack P ($P = \xi f$) can be calculated.

The fatigue crack is modelled by a circular ring heat source located in the reverse plastic zone at the crack tip whose radius increases with time.

From the heat transfer equation and considering adiabatic conditions on the surface of the specimen, and normalizing dimensions in the problem, the evolution of the non-dimensional temperature during the fatigue testing can be obtained.

The numerical resolution of the thermal problem allows the determination of the evolution of the temperature field with time in the specimen. The comparison between test and model shows a good correlation (Fig. 8). In particular, the propagation duration of the crack is well estimated by the model.

So, the increase in temperature at the end of the experimental test corresponds to the fracture initiation, and the number of cycles at initiation can be determined accurately. The number of cycles at the crack initiation (Fig. 8) corresponds to a temperature increase of 0.07 °C (noise of camera after filtration of temperature signal for an aperture time of 10 μs).

For our materials, the results of the number of cycles at initiation N_i and the ratio of N_i over N_f (number of cycles at fracture) is given in Table 3. These results confirm that in the gigacycle domain, more than 92% of the total life

Table 3 Number of cycles at initiation and comparison with Paris' model for fish-eye propagation

Alloy	N_i	N_f	N_i/N_f	Localization	$N_f - N_i$	N_{prop}
AlSi7Mg06	8.1010×10^6	8.6932×10^6	0.932	Surface	5.92×10^5	–
	8.0826×10^6	8.3276×10^6	0.971	Surface	2.45×10^5	–
	1.15310×10^7	1.25132×10^7	0.922	Surface	9.82×10^5	–
AlSi5Cu3Mg	7.89184×10^7	8.11392×10^7	0.973	Fish eye	2.23×10^6	2.73×10^6
AISI 4240 ($T = 430$ °C)	3.05×10^5	3.3094×10^5	0.922	Surface	2.6×10^4	–
AISI 4240 ($T = 610$ °C)	1.76155×10^7	1.76197×10^7	0.998	Surface	4.2×10^3	–
AISI 5120	8.3620×10^7	8.3700×10^7	0.999	Fish eye	0.8×10^5	6.16×10^5

$E_{AlSi5Cu3Mg} = 72560$ MPa, $E_{AISI5120} = 210000$ MPa

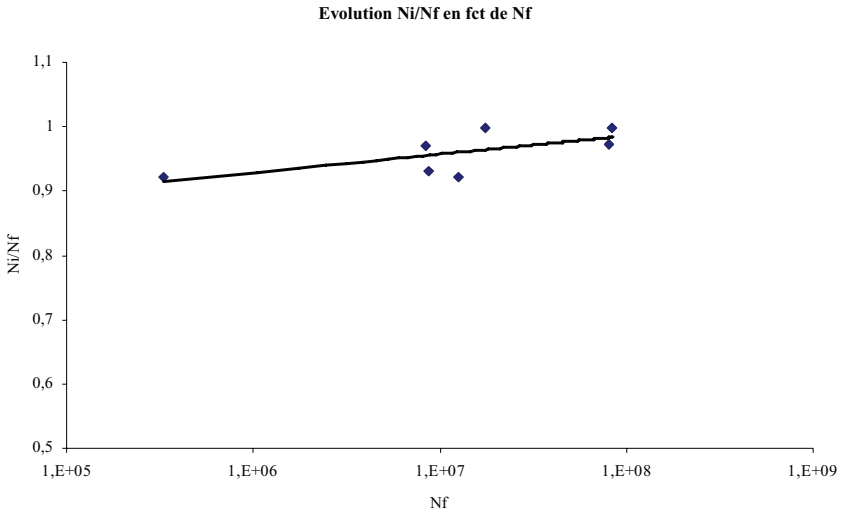

Fig. 9 N_i/N_f evolution versus N_f for the studied materials.

is devoted to the initiation of the crack. Figure 9 shows the relation between N_i/N_f versus N_f, and the portion of the total life devoted to the initiation increases with the number of cycles to failure. The greater the number of cycles to fracture, the larger the part of total life for initiation of the crack. Consequently, the number of cycles for the propagation of the fish eye is weak and the comparison (Table 3) of the Paris model with our experiments is good.

CONCLUSION

The final goal of this research is to understand the damage mechanism inside the metal, around defects, when the fatigue life reaches 10^9. Of course, it is experimentally difficult to catch observations at 10^9 cycles. In order to approach this objective, the experimental study has been carried out for a fatigue range between 10^6 and 10^9. Further to this, an analytical model has been derived from the Paris law.

A temperature measurement with an infrared camera was performed during fatigue tests on a piezoelectric fatigue machine on cast aluminium–silicon alloys and three low alloyed steels. Different stress levels were applied. At the beginning of the test, the temperature rapidly increases, followed by a stabilization. The higher the applied stress, the larger the increase in temperature and the more significant the energy dissipated. At the end of the test, the temperature increases very rapidly until the fracture.

The numerical resolution of the thermal problem allows the determination of the evolution of the temperature field with time in the specimen. The comparison between test and model shows a good correlation, and the sudden increase of the temperature allows to determine the cycle number at crack initiation and it proves that more than 92% of the total life is devoted to the initiation of the crack.

The portion of the total life devoted to the initiation increases with the number of cycles to failure. When the initiation is subsurface and leads to a fish-eye formation, the

simplified Paris model allows a prediction of the number of cycles to fish eye formation. To conclude, it is proven that the key damage in VHCF is initiation and not slow crack propagation.

REFERENCES

1 Bathias, C. and Paris, P. C. (2005) *Gigacycle Fatigue in Mechanical Practice*. Marcel Dekker, New York.

2 Mughrabi, H. (2006) Specific features and mechanisms of fatigue in the ultrahigh-cycle regime. *Int. J. Fatigue* **28,** 1501–1508.

3 Paris, P. C., Marines-Garcia, I., Hertzberg, R. W. and Donald, J. K. (2004) The relationship of effective stress intensity factor, elastic modulus and Burger's-vector on fatigue crack growth as associated with "Fish Eye" gigacycle fatigue phenomena. *Proceedings of the Third International Conference on Very High Cycle Fatigue (VHCF-3)*, *Kyoto*, *Japan*, pp. 16–19.

4 Marines-Garcia, I., Paris, P. C., Tada, H. and Bathias, C. (2006) Fatigue crack growth from small to large cracks in gigacycle fatigue with fish-eyes failure. *9th International Fatigue Congress*, *Atlanta*, *Georgia*, *USA*.

5 Marines-Garcia, I., Paris, P. C., Tada, H. and Bathias, C. (2007) Fatigue crack growth from small to long cracks in VHCF with surface initiations. *Int. J. Fatigue* **29,** 2072–2078.

6 Ranc, N., Wagner, D. and Paris, P. C. (2008) Study of thermal effects associated with crack propagation during very high cycle fatigue. *Acta Materiala* **56,** 4012–4021.

7 Luong, M. P. (1998) Fatigue limit evaluation of metals using an infrared thermographic technique. *Mech. Mater.* **28,** 155–163.

8 Liaw, P. K., Wang, H., Jiang, L., Yang, B., Huang, J. Y., Kuo, R. C. and Huang, J. G. (2000) Thermographic detection of fatigue damage of pressure vessel steels at 1,000 Hz and 20 Hz. *Scripta. Mater.* **42,** 389–395.

9 Yang, B., Liaw, P. K., Wang, H., Jiang, L., Huang, J. Y., Kuo, R. C. and Huang, J. G. (2001) Thermographic investigation of the fatigue behavior of reactor pressure vessel steels. *Mat. Sci. Eng. A* **314,** 131–139.

10 Fargione, G., Geraci, A., La Rosa, G. and Risitano, A. (2002) Rapid determination of the fatigue curve by the thermographic method. *Int. J. Fatigue* **24,** 11–19.

11 Curà, F., Curti, G. and Sesana, R. (2005) A new iteration method for the thermographic determination of fatigue limit in steels. *Int. J. Fatigue* **27,** 453–459.

12 Boulanger, T., Chrysochoos, A., Mabru, A. and Galtier, A. (2004) Calorimetric analysis of dissipative and thermoelastic effects associated with the fatigue behavior of steels. *Int. J. Fatigue* **26,** 221–229.

13 Meneghetti, G. (2007) Analysis of the fatigue strength of a stainless steel based on the energy dissipation. *Int. J. Fatigue* **29,** 81–84.

14 Morabito, A. E., Chrysochoos, A., Dattoma, V. and Galietti, U. (2007) Analysis of heat sources accompanying the fatigue of 2024 T3 aluminium alloys. *Int. J. Fatigue* **29,** 977–984.

15 Beghi, M., Bottani, C. E. and Caglioti, G. (1984) Temperature variations around the crack tip during fracture test. Italy-Switzerland workshop, Lugano, 24–25 May.

16 Harvey II, D. P., Bonenberger, R. J. and Wolla, J. W. (1998) Effects of sequential cyclic and monotonic loadings on damage accumulation in nickel 270. *Int. J. Fatigue* **4**, 291–300.

17 Mason, W. P. (1950) *Piezoelectronic Crystals and their Application*. Ultrasonics, Van Nostrand, New York.

18 Wu, T. Y., Ni, J. G. and Bathias, C. (1993) Automatic in Ultrasonic Fatigue Machine to Study Low Crack Growth at Room and High Temperature. *ASTM STP* **1231,** 598–607.

19 Bathias, C. and Ni, J. G. (1993) Determination of Fatigue Limit between 10^5 and 10^9 cycles using an Ultrasonic Fatigue Device. *ASTM STP* **1211,** 151–152.

20 Bathias, C. and Pineau, A. (2008) *Fatigue des matériaux et des structures*. Lavoisier, France.

21 Sakai, T. (2007) Review and prospects for current studies on very high cycle fatigue of metallic materials for machine structural use. *Fourth International Conference on Very High Cycle Fatigue (VHCF-4)*, *TMS (The Minerals, Metals& Materials Society)*, pp. 3–12.